OSSE Assessment of Underwater Glider Arrays to Improve Ocean Model Initialization for Tropical Cyclone Prediction

GEORGE R. HALLIWELL JR. AND GUSTAVO J. GONI

NOAA/AOML/Physical Oceanography Division, Miami, Florida

MICHAEL F. MEHARI

Cooperative Institute for Marine and Atmospheric Studies, University of Miami, and NOAA/AOML/Physical Oceanography Division, Miami, Florida

VILLY H. KOURAFALOU

Rosenstiel School of Marine and Atmospheric Science, University of Miami, Miami, Florida

MOLLY BARINGER AND ROBERT ATLAS

NOAA/Atlantic Oceanographic and Meteorological Laboratory, Miami, Florida

(Manuscript received 2 November 2018, in final form 2 October 2019)

ABSTRACT

Credible tropical cyclone (TC) intensity prediction by coupled models requires accurate forecasts of enthalpy flux from ocean to atmosphere, which in turn requires accurate forecasts of sea surface temperature cooling beneath storms. Initial ocean fields must accurately represent ocean mesoscale features and the associated thermal and density structure. Observing system simulation experiments (OSSEs) are performed to quantitatively assess the impact of assimilating profiles collected from multiple underwater gliders deployed over the western North Atlantic Ocean TC region, emphasizing advantages gained by profiling from moving versus stationary platforms. Assimilating ocean profiles collected repeatedly at fixed locations produces large root-mean-square error reduction only within ~50 km of each profiler for two primary reasons. First, corrections performed during individual update cycles tend to introduce unphysical eddy structure resulting from smoothing properties of the background error covariance matrix and the tapering of innovations by a localization radius function. Second, advection produces rapid nonlinear error growth at larger distances from profiler locations. The ability of each individual moving glider to cross gradients and map mesoscale structure in its vicinity substantially reduces this nonlinear error growth. Glider arrays can be deployed with horizontal separation distances that are 50%–100% larger than those of fixed-location profilers to achieve similar mesoscale error reduction. By contrast, substantial larger-scale bias reduction in upper-ocean heat content can be achieved by deploying profiler arrays with separation distances up to several hundred kilometers, with moving gliders providing only modest additional improvement. Expected sensitivity of results to study region and data assimilation method is discussed.

1. Introduction

Short-term ocean prediction using numerical general circulation models is important for a variety of applications that include transport and dispersion of marine debris and oil, search and rescue, and coupled tropical cyclone (TC) prediction. For TC prediction, the ocean model must accurately forecast sea surface temperature (SST) beneath storms to correctly predict enthalpy flux from ocean to atmosphere, and hence intensity evolution. Accurate ocean model initialization is necessary to avoid large errors in predicted SST (Halliwell et al. 2008, 2011). The next generation of coupled prediction systems to be run at the NOAA/NCEP Environmental Modeling Center (EMC), such as the Hurricane Weather Research and Forecasting Model (HWRF) and the Hurricane Multiscale, Ocean-Coupled, Nonhydrostatic (HMON) model, will use a data-assimilative ocean analysis product for initialization, specifically the Real-Time Ocean

Corresponding author: George R. Halliwell Jr., george.halliwell@noaa.gov

DOI: 10.1175/JTECH-D-18-0195.1

Forecast System (RTOFS; http://www.polar.ncep.noaa.gov/global/). Ocean observing systems will therefore play an important future role in providing accurate initial ocean fields for TC prediction.

The assimilation of existing global observing systems designed primarily for long-term ocean monitoring into data-assimilative ocean general circulation models already provides substantial error reduction in ocean analysis products that will benefit TC prediction and other applications (e.g., Goni et al. 2009; Oke et al. 2015; Turpin et al. 2016). Key existing observing systems include satellite altimetry, satellite and in situ SST, Argo profiling floats, expendable bathythermographs (XBTs) deployed from research and cargo ships, and moorings. Because significant errors and biases still remain in analysis products that assimilate these observations, attention is given to supplementing the existing global observing system with enhanced regional ocean observations to further reduce initialization errors.

For TC intensity prediction, initial ocean fields must not have significant upper-ocean warm or cold biases. Furthermore, these initial fields must accurately resolve the three-dimensional structure of ocean mesoscale eddies and boundary currents because the background vorticity associated with these features affects the magnitude and pattern of SST cooling forced by storms (e.g., Shay et al. 2000; Jacob and Shay 2003; Wu et al. 2007; Jaimes and Shay 2009; Ma et al. 2013; Jaimes et al. 2011, 2015, 2016). It is also important to correctly initialize differences in the temperature, salinity, and density stratification associated with these ocean features. Currently, satellite altimetry is the only component of the global observing system designed to resolve the horizontal structure of mesoscale ocean features (e.g., Verrier et al. 2017). However, the large cross-track separation distance for individual altimeters limits their ability to correct mesoscale structure over the smaller horizontal scales resolved by contemporary ocean forecast models. Satellite and in situ SST observing platforms are important in this regard, but provide limited temperature correction beneath the mixed layer. This is especially true during hurricane season when horizontal SST structure is substantially decoupled from the underlying mesoscale eddy structure (e.g., Scharroo et al. 2005). Argo floats correct temperature and salinity distributions over the upper 2000 m over large horizontal scales, but when used alone, space–time sampling is inadequate to resolve the ocean mesoscale. XBT and mooring measurements alone are also not designed to correctly resolve mesoscale variability for short-term ocean forecast applications such as TC intensity forecasts. Supplemental subsurface ocean observations hold the promise of filling these observational gaps.

One approach under consideration to improve the three-dimensional representation of temperature and salinity in hurricane-prone ocean regions is to deploy arrays of underwater gliders during TC season over predefined ocean region where storms are known to intensify. Prototype deployments of underwater gliders during hurricane season have been conducted near Puerto Rico since 2014, originally with one glider deployed north of, and another deployed south of, the island (Domingues et al. 2015). The glider located north of Puerto Rico during Hurricane Gonzalo (2014) demonstrated the capability of monitoring prestorm ocean conditions and the ocean response forced by this storm (Dong et al. 2017). To justify the deployment of underwater glider arrays, it is important to demonstrate significant positive impact on reducing ocean analysis and forecast errors, and also to evaluate different deployment strategies with the goal of designing a viable operational glider network. Particular attention is paid to the additional positive impact achieved by assimilating profiles collected by moving gliders versus profiles from stationary platforms.

Idealized observing system simulation experiments (OSSEs) are performed during the 2014 Atlantic hurricane season over the western North Atlantic Ocean and analyzed to quantitatively assess the positive impact of deploying an array of piloted gliders in comparison to deploying stationary platforms. The dependence of positive impacts on platform type and horizontal spacing is quantified based on root-mean-square error (RMSE) and bias reduction. The extent to which moving gliders can be deployed at coarser resolution than stationary platforms to achieve the same levels of RMSE and bias reduction is documented. Factors responsible for the superior performance of moving platforms are explored. Results presented herein are strictly valid only for the specific region studied and only for the specific OSSE system used, which includes the ocean model and data assimilation (DA) method. The present study must be considered an initial documentation of the additional positive impact achieved by assimilating profiles from moving gliders compared to stationary platforms.

A brief description of the OSSE system that includes recent changes is presented in section 2. Analysis methods and experimental design are discussed in section 3. A reevaluation of the OSSE system to assess the impact of recent system configuration changes is presented in section 4. The ability of a network of moving gliders to more effectively correct ocean mesoscale variability compared to an array of stationary platforms, along with an analysis of responsible factors, is presented in section 5. The impacts of both moving and stationary platforms are quantitatively assessed and compared in section 6 with respect to improving the representation of the ocean mesoscale and correcting large-scale model bias

in upper-ocean temperature. Conclusions are presented in section 7.

2. Ocean OSSE system

a. *OSSE method*

OSSE systems provide the means to quantitatively assess impacts on analyses and forecasts of new observing systems and impacts of different deployment strategies for existing systems (e.g., Atlas 1997; Atlas and Riishojgaard 2008; Hoffman and Atlas 2015). An OSSE system consists of 1) a ''Nature Run'' (NR), that is, a data-validated, free-running model that represents the ''truth'' with respect to the processes being forecast; 2) a data-assimilative ocean forecast system that couples a different ocean model [the ''Forecast Model'' (FM)] to an ocean DA system; and 3) software to simulate ocean observations from the NR containing realistic errors for assimilation into the forecast system.

OSSEs are an extension of observing-system experiments (OSEs). OSEs involve twin data denial numerical experiments to quantitatively assess the impact of existing observing systems. Impacts must be assessed versus observations withheld from assimilation or analysis products derived from observations. OSSEs follow the same procedures as OSEs but assimilate synthetic observations simulated from the NR. Impacts can then be assessed by comparing the FM experimental analyses to the high-resolution three-dimensional representation of the truth provided by the NR. Therefore, OSSE systems cannot only assess new observing systems and strategies, but also assess the impacts of existing observing systems more thoroughly than is possible with OSEs. OSSEs also have an advantage over linearized procedures to assess impact, such as adjoint methods, because the influence of nonlinear processes on observing-system impact can be documented. It is demonstrated herein that nonlinear advection of thermodynamical fields exerts a large influence on observing-system impacts.

The present ocean OSSE system employs the fraternal twin approach, with two substantially different configurations of the Hybrid Coordinate Ocean Model (HYCOM; Bleck 2002; Chassignet et al. 2003, 2007; Halliwell 2004) used for the NR and FM. The OSSE system design and evaluation procedures follow strict guidelines developed originally for atmospheric OSSE systems to ensure that credible impact assessments are obtained (Atlas 1997; Hoffman and Atlas 2015). To ensure that realistic errors exist between the FM and NR, they are run with altered numerical schemes, subgrid-scale parameterizations, and different horizontal and vertical resolution (Table 1). These configurations are designed so that the NR is more realistic than the FM, a key requirement of a credible OSSE system (Atlas 1997; Hoffman and Atlas 2015). Consistent with this choice, parameters are set to make the FM more diffusive than the NR, and thus more representative of older-generation ocean models. The FM is run at lower resolution than the NR, 0.08° Mercator mesh and 26 vertical layers versus 0.04° Mercator mesh and 35 vertical layers. The choice of Mercator mesh results in grid resolution that increases with latitude in a manner consistent with the meridional decrease in Rossby radius of deformation associated with planetary vorticity.

The ocean OSSE system used in this work was initially set up and evaluated in the Gulf of Mexico (Halliwell et al. 2014). Halliwell et al. (2015) evaluated the impact of different airborne ocean profile survey strategies on analyses and forecasts in the Gulf of Mexico during the *Deepwater Horizon* oil spill, extending results from the OSE analysis of the real airborne surveys presented in a previous work (Shay et al. 2011). The OSSE system has since been expanded into a larger Atlantic Ocean domain (from 5°S to 45°N, extending east to 20°W). The rigorous validation of the NR for this expanded system is presented in Kourafalou et al. (2016) and Androulidakis et al. (2016). Halliwell et al. (2017a) documented the credibility of the full North Atlantic OSSE system by performing OSE–OSSE comparison experiments. Halliwell et al. (2017a) then use the system to quantitatively assess the impact of synthetic ocean profiles collected by Argo floats and of the deployment of underwater gliders. Using the North Atlantic system, Halliwell et al. (2017b) evaluate the impact of different airborne ocean profile survey strategies on ocean analyses prior to Hurricane Isaac (2012) in the Gulf of Mexico, and also prior to Hurricanes Edouard (2014) and Gonzalo (2014) in the open Atlantic Ocean. The overarching conclusion from these OSSE studies was that for an individual surve multiple ocean profilers must be deployed at sufficiently high horizontal resolution [$O(1°)$ or less] to significantly reduce errors in mesoscale structure over the correction already realized by assimilating satellite altimetry. Furthermore, deployments should cover as much area as possible because correction of mesoscale structure is tightly confined to the region sampled.

Two significant changes have been made to the OSSE system for the present analysis. First, data from the Prediction and Research Moored Array in the Tropical Atlantic (PIRATA) ocean moorings are now being assimilated. Because these moorings are located in the far eastern part of the North Atlantic OSSE domain and far removed from the region analyzed herein, they are not considered further. Second, the vertical mixing algorithm used by the FM was changed. In previous OSSE work, both the NR and FM used the *K*-profile parameterization

TABLE 1. Configuration differences between the NR and FM of the fraternal twin OSSE system.

Model attribute	Nature Run model (HYCOM)	OSSE system Forecast Model (HYCOM)
Horizontal resolution	0.04° Mercator (1951 × 1387)	0.08° Mercator (976 × 694)
Vertical discretization	Hybrid; 35 layers (2000-m reference pressure)	Hybrid; 26 layers (0-m reference pressure)
Time steps (baroclinic/barotropic)	180/6 s	240/4 s
Bathymetry	New, 0.04° product from the Naval Research Laboratory	0.08° bathymetry from HYCOM Atlantic climatological run
Atmospheric forcing	U.S. Navy NOGAPS model (every 3 h)	Navy NOGAPS model (every 6 h)
Initial and boundary conditions	Global HYCOM (interpolated to higher-resolution NR mesh)	HYCOM Atlantic climatological simulation
Thermobaric pressure gradient correction	Yes	No
Vertical mixing algorithm	*K*-profile parameterization	Mellor–Yamada level 2.5
Min mixed layer thickness	10 m	12 m
Quadratic bottom friction coef	0.0023	0.0032
Diffusion velocity for Laplacian viscosity	0.002 86	0.0044
Diffusion velocity for biharmonic viscosity	0.02	0.03
Diffusion velocity for biharmonic thickness diffusion	0.01	0.017
Diffusion velocity for Laplacian scalar diffusion	0.0050	0.0087
Hybrid grid generator vertical remapping algorithm	Weighted essentially nonoscillatory (WENO)-like	Piecewise linear mapping
Hybrid grid generator inverse relaxation coef	One baroclinic time step	Four baroclinic time steps

(KPP; Large et al. 1994) with different parameter choices (Halliwell et al. 2017a). In the present study, The Mellor–Yamada level-2.5 mixing model (MY; Mellor and Yamada 1982) replaces the KPP model. This change was motivated by the desire to further improve another key requirement of OSSE systems, specifically that errors between the FM and NR must be similar in magnitude to errors between the NR and the true ocean (Atlas 1997; Hoffman and Atlas 2015). In the previous system configuration, errors between the FM and NR were somewhat smaller than required, although not by a sufficiently large margin to invalidate OSSE results (Halliwell et al. 2017a). The present change of mixing model was intended to increase errors between the models. Because of these configuration changes, the OSSE system is reevaluated herein using OSE–OSSE comparisons (section 4) prior to presenting impact assessments.

b. DA method

The data assimilation system uses the statistical optimum interpolation approach, and is designed specifically to assimilate state variables (temperature T, salinity S, and layer thickness) into the Lagrangian vertical coordinate structure of HYCOM (Halliwell et al. 2014). Along-track SSH anomalies from satellite altimetry are assimilated by correcting vertical profiles of layer thickness so that water mass properties are preserved following Cooper and Haines (1996). All temperature–salinity profiles are assimilated after first remapping them from z coordinates into the model hybrid vertical coordinate discretization. For profiles that measure temperature alone, corresponding salinity profiles based on climatological T–S correlations are generated prior to the vertical remapping. SST is assimilated only within the upper two model layers, which always remain within the mixed layer.

The background error covariance for the DA system is obtained from a decade-long unconstrained simulation by the FM. Covariances are calculated separately for each month as described in Halliwell et al. (2014) to primarily resolve mesoscale structure, and not the larger horizontal scales of the seasonal cycle present in upper-ocean fields. Increments for each individual observation are tapered by the Gaussian-like Gaspari and Cohn (1999) localization function that equals one at the observation location, and then decreases to zero at a prespecified radial distance from the observation. This radius is chosen to be 200 km in the present analysis, and the suitability of this choice is justified later. All data-assimilative experiments are performed as described in Halliwell et al. (2014, 2017a) using a daily update cycle. Special considerations with respect to assimilating profiles from moving gliders are described later.

3. Procedures

a. Analysis approach

Six model fields highly relevant to the TC prediction problem are analyzed. The structure of the pressure field associated with surface quasigeostrophic currents is

TABLE 2. Experiments performed for the OSSE system evaluation. Argo profiles were withheld from all experiments for evaluation. Here, GOFS is the Global Ocean Forecasting System.

Expt	Observing systems assimilated	Run interval	Initialization
FM	None (unconstrained)	From 1 Oct 2008 through 2017	GOFS global HYCOM analysis
CONTROL	Three altimeters (*CryoSat-2*, *Jason-2* plus *Jason-3*, and *SARAL*); SST; XBT; PIRATA moorings	From 1 Jan 2014 through 2017	FM
2ALT	Two altimeters (*CryoSat-2* and *Jason-2* plus *Jason-3*); SST; XBT; PIRATA moorings	From 1 Jan 2014 through 2017	FM
1ALT	One altimeter (*CryoSat-2*); SST; XBT; PIRATA moorings	From 1 Jan 2014 through 2017	FM
NOALT	SST; XBT; PIRATA moorings	From 1 Jan 2014 through 2017	FM
NOSST	Three altimeters (*CryoSat-2*, *Jason-2* plus *Jason-3*, and *SARAL*); XBT; PIRATA moorings	From 1 Jan 2014 through 2017	FM

represented by dynamic height at the surface relative to 1000 m D_{1000}. The structure of this field within the analysis domain is dominated by mesoscale eddies. Mesoscale structure is also represented by the 20°C isotherm depth H_{20}, which is closely associated with main thermocline depth. To assess impacts on upper-ocean thermal structure, one surface field (SST) and two subsurface fields (temperature at 100 m T_{100} and temperature averaged between the surface and 100 m $T_{0–100}$) are analyzed. While SST tends to be decoupled from the subsurface structure of mesoscale features in the tropical ocean during hurricane season, both T_{100} and $T_{0–100}$ substantially reflect thermal structure beneath the surface mixed layer associated with mesoscale features. Price (2009) recommended $T_{0–100}$ as a proxy of expected SST cooling by TC forcing under the assumption of maximum vertical mixing, and therefore as an indicator of intensification potential. Sea surface salinity (SSS) is also analyzed.

Impacts are assessed based on reduction in both RMSE and bias magnitude. Error fields gridded on the model mesh are defined as the difference fields between the experiment under consideration and the truth represented by the NR. Because RMSE is calculated after removing mean values from the fields within the analysis domain, it predominantly represents the fidelity with which mesoscale variability is represented in the analyses. To further analyze the impact of observations on correcting mesoscale structure, power spectrum analysis is performed in zonal and meridional wavenumber space.

b. Experiments for OSSE system evaluation

A set of identical OSE–OSSE twin experiments was performed over the full North Atlantic domain for the evaluation (Table 2), with the unconstrained FM experiment serving as reference. The remaining experiments (CONTROL, 2ALT, 1ALT, NOALT, and NOSST) were run in both of the OSE (real observations) and OSSE (synthetic observations) frameworks with Argo profiles, actual ones for OSE and synthetic ones for OSSE, withheld for evaluation. All synthetic data for the OSSEs are simulated from the NR at the same locations, depths, and times as the real data. Table 3 lists all synthetic observations simulated from the NR that are assimilated and summarizes the realistic errors added to them. Experiment CONTROL assimilated the components of the global observing system listed in Table 2. For altimetry, CONTROL assimilated three continuous altimeter records from 2014 through 2017: *CryoSat-2*, *Jason-2* plus *Jason-3*, and the Ka-band altimeter from *Satellite with Argos and AltiKa* (*SARAL*). For the OSE and OSSE data denial experiments, 2ALT denied *SARAL*, 1ALT denied *Jason-2* plus *Jason-3* and *SARAL*, NOALT denied all altimeters, and NOSST denied all SST (Table 2). These experiments were all run from 1 January 2014 through 31 October 2017.

c. Idealized experiments for impact assessment

Although all experiments are conducted over the full North Atlantic OSSE domain (from 5°S to 45°N, extending east to 20°W), instrument deployments and analyses for the idealized experiments are conducted within a smaller 15° by 15° box in the western Atlantic Ocean TC region situated south of the Gulf Stream and north of the Caribbean islands (Fig. 1). This box spans the interior region of the Subtropical Gyre, and is sufficiently large to permit rigorous statistical analysis of observing-system impacts over a region where mesoscale eddy statistics are quasi-homogeneous. Within the analysis box, stationary platforms are deployed on six sets of grid points with horizontal separation distances of 0.5°, 1.0°, 2.0°, 3.5°, 4.7°, and 7.0° in both latitude and longitude. The 2.0° grid is shown in Fig. 1 while the others grids share the same four corner points. Gliders are released at the same locations as the stationary platforms and move along ladder-shaped tracks in a reverse figure-8 sense as shown in Fig. 1. The area sampled by each glider

TABLE 3. List of synthetic observations assimilated with added errors.

Observing System	Instrument	Instrument measurement RMS error	RMS representation errors	Other RMS errors	Localization radius
Satellite altimetry	CryoSat	0.02 m	0.02 m; correlation length scale 40 km	Internal tides 0.01 m (length scale 5 km)	225 km
	Jason-2 and *Jason-3*	0.02 m	0.02 m; correlation length scale 40 km	Internal tides 0.01 m (length scale 5 km)	225 km
	SARAL	0.02 m	0.02 m; correlation length scale 40 km	Internal tides 0.01 m (length scale 5 km)	225 km
	Haiyang-2a	0.02 m	0.02 m; correlation length scale 40 km	Internal tides 0.01 m (length scald 5 km)	225 km
SST	Satellite multichannel SST	0.3°C	0.2°C		80 km
	In situ stationary surface buoy	0.1°C	0.2°C		80 km
	In situ surface drifter	0.1°C	0.2°C		80 km
	In situ ship intake	0.2°C	0.2°C		80 km
Argo	Argo profiling floats	*T*: 0.005°C; *S*: 0.005 practical salinity units (psu)	*T*: 0.15°C; *S*: 0.08 PSU (taper to zero from surface to 200 m)	Depth error: 2 m (taper to zero above 100 m)	200 km
XBT	Primarily ship transects	0.05°C	0.2°C (taper to zero from surface to 200 m)	Depth error: 1.5% of depth fall rate	200 km
Ocean Moorings	PIRATA moorings				
Gliders	Idealized arrays	Same as Argo	Same as Argo	Same as Argo	200 km
Stationary profilers	Idealized arrays	Same as Argo	Same as Argo	Same as Argo	200 km

FIG. 1. Analysis domain box for the idealized experiments shown within a subset of the full North Atlantic model domain. Stationary profilers and gliders were released at longitude–latitude grid points with separation distances of 0.5°, 1.0°, 2.0° (shown), 3.5°, 4.7°, and 7.0°, all sharing common corner points. All gliders released at these points executed a reverse figure-eight pattern over a track spanning 2° longitude and latitude, as shown on the inset at right, while traveling at 0.25 m s^{-1}. Gliders were not released at 0.5° resolution; the gliders released with 1° separation followed a track spanning 1° longitude and latitude.

is approximately centered around the release point. Gliders are not released at a separation distance of 0.5° because that separation would, in principle, require an unrealistic number of gliders to cover a sufficiently large ocean area to significantly impact TC intensity prediction. The 0.5° separation is retained for stationary platforms because it matches separation distances of airborne profiler surveys that were quantitatively assessed in earlier OSSE studies (Halliwell et al. 2015, 2017b), permitting comparison with the earlier results.

All idealized experiments are listed in Table 4. The same unconstrained FM experiment used in the OSSE system evaluation (Table 2) again serves as a reference for these idealized experiments. Experiment CONTROL is run from 1 January through 31 October 2014 and assimilates synthetic observations from major components of the existing ocean observing system, specifically satellite altimetry, satellite and in situ SST, Argo floats, XBT profiles, and PIRATA moorings. The remaining experiments are run from 1 May through 31 October 2014 and are initialized by the FM (OSE) and CONTROL (OSSE). They assimilate either single daily synthetic profiles from stationary platforms or multiple daily synthetic profiles from moving underwater gliders. Four sets of experiments are then run assimilating gliders only (experiments G1.0–G7.0); fixed-location profilers only (experiments F0.5–F7.0); gliders added to CONTROL (experiments CG1.0–CG7.0); and stationary profilers added to CONTROL (CF0.5–CF7.0) (Table 4).

TABLE 4. Idealized experiments performed for the impact assessments.

Expt	Observing systems assimilated	Run interval	Initialization
FM	None (unconstrained)	From 1 Oct 2008 through 2017	GOFS global HYCOM analysis
CONTROL	Four altimeters (*CryoSat-2*, *Jason-2*, *Haiyang-2A*, and *SARAL*); SST; Argo; XBT; PIRATA moorings	1 Jan 2014–31 Oct 2014	FM
G1.0 G2.0 G2.0D G3.5 G4.7 G7.0	Underwater gliders only; multiple horizontal separation distances from 1.0° to 7.0°; expt G2.0D follows G2.0 but assimilates only one profile per day	1 May 2014–31 Oct 2014	FM
F0.5 F1.0 F2.0 F3.5 F4.7 F7.0	Stationary profilers only; multiple horizontal separation distances from 0.5° to 7.0°	1 May 2014–31 Oct 2014	FM
CG1.0 CG2.0 CG3.5 CG4.7 CG7.0	CONTROL plus underwater gliders; multiple horizontal separation distances from 1.0° to 7.0°	1 May 2014–31 Oct 2014	CONTROL
CF0.5 CF1.0 CF2.0 CF3.5 CF4.7 CF7.0	CONTROL plus stationary profilers; multiple horizontal separation distances from 0.5° to 7.0°	1 May 2014–31 Oct 2014	CONTROL

Motion and sampling characteristics of the synthetic gliders are designed to mimic the properties of actual gliders (Domingues et al. 2015). In our numerical experiments, gliders sample 12 temperature–salinity profiles per day (the maximum number that can be realistically achieved) over the upper 1000 m with a vertical resolution of 4 m. Each glider navigates along its path at a speed of 0.25 m s^{-1}, spanning 2–3 model grid points per day. To reduce the number of profiles assimilated, all daily profiles within a single model grid box are averaged together, resulting in 2–3 daily profiles. Daily profiles of temperature and salinity over the upper 1000 m from stationary platforms are sampled at the same vertical resolution of 4 m. The same errors are added to the synthetic profiles from both platforms (Table 3), which ensures that impact differences will result only from glider motion and the multiple daily profiles that are collected by this platform.

4. OSSE system evaluation

RMSE and bias in the six analyzed model fields were calculated over the time interval 15 July–15 October for the years 2014–17, spanning the peak of these four hurricane seasons in the region of study. Field values were calculated from all Argo profiles, real for OSE and synthetic for OSSE, that were located in the subset of the North Atlantic domain spanning from 7.5° to 40.5°N and extending east to 40°W during the time windows above. The same field values were calculated from the model experiments at Argo float locations to be directly compared to values calculated from real Argo (OSE) and synthetic Argo (OSSE) profiles. RMSE was then calculated separately for OSE and OSSE experiments over all real (OSE) and synthetic (OSSE) Argo profiles.

RMSE from the six evaluation experiments (Table 2) for the six model fields are presented for both the OSE and OSSE experiments (Fig. 2). The large RMSE values for FM serve as the benchmark to measure impacts of assimilation. OSSE RMSE values from the FM are similar in magnitude, but slightly smaller than, the corresponding OSE values for all fields except SSS, where the FM substantially underestimates SSS variability. This result confirms that, except for SSS, errors in the FM with respect to the NR are similar to errors between the FM and the true ocean, verifying a key requirement of credible OSSE systems. This similarity in error magnitudes is a modest improvement over the previous configuration of the OSSE system (Halliwell et al. 2017a) produced by the FM configuration change.

Overall, RMSE reduction is qualitatively similar between the OSEs and OSSEs. For H_{20}, the OSE results

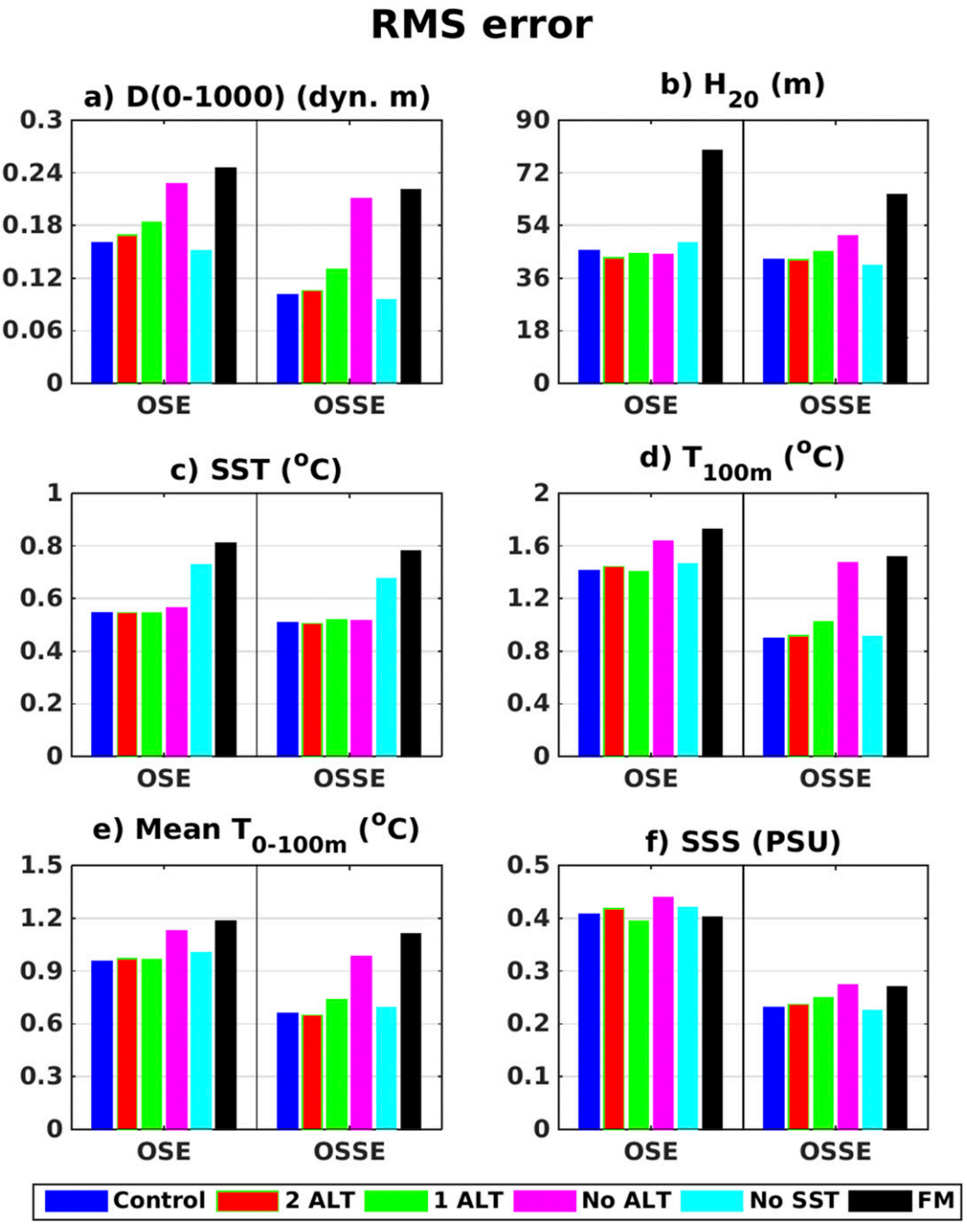

FIG. 2. Results from OSE–OSSE twin comparison experiments for six model fields from the seven multiyear experiments listed in the legend at the bottom. Errors were calculated during the height of four hurricane seasons (15 Jul–15 Oct 2014–17).

show larger impacts. For the remaining variables, the OSSE results show equal or larger impacts. With Argo profile data withheld, assimilation produces little impact toward improving SSS in both OSEs and OSSEs, an agreement that holds despite the FM underestimate of SSS variance. The previous configuration of the OSSE system tended to overestimate impacts by 10%–15%. Present results reveal a similar overestimate on average. This overestimate is sufficiently small to not alter the fundamental results of analyses presented herein. The fact that relative OSE and OSSE impacts differ for different model fields (Fig. 2) demonstrates that impacts must be assessed using multiple model fields to provide credible assessments.

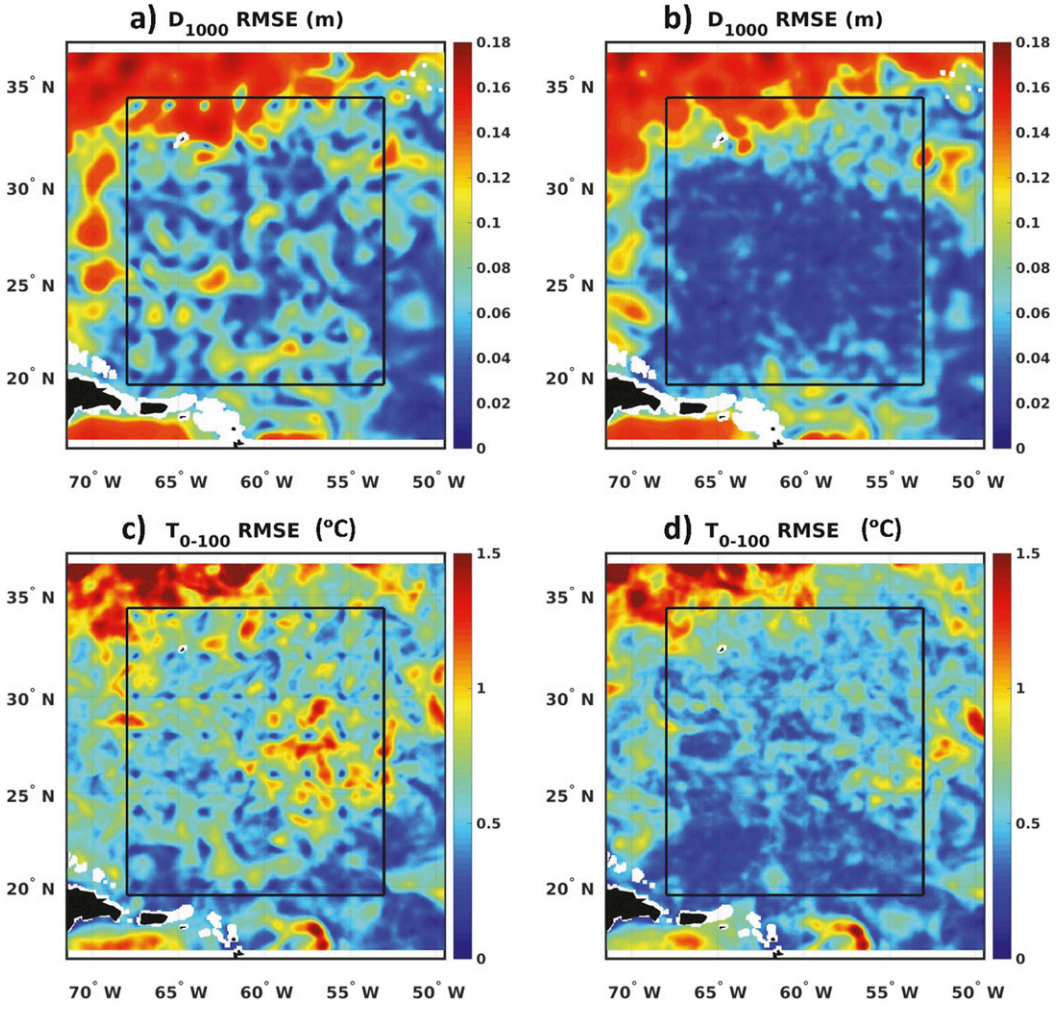

FIG. 3. Maps of RMSE over a subdomain containing the analysis box for experiments (left) F2.0 and (right) G2.0 for (a),(b) D_{1000} and (c),(d) $T_{0–100}$. Statistics are calculated over the time interval 1 Jul–12 Oct 2014.

5. Impact of platform type on reducing RMSE

a. Impact on radius of influence

Maps of RMSE over a subdomain containing the analysis box calculated over 1 July–12 October 2014 are presented for D_{1000} and $T_{0–100}$ from experiment F2.0 (Figs. 3a,c) and from experiment G2.0 (Figs. 3b,d). Given that impact assessments herein are based on the ability to reduce both RMSE and large-scale bias in prestorm ocean conditions, the time window is terminated on 12 October because Hurricane Gonzalo forced a large ocean response that significantly affected the statistics. When profiles from stationary platforms are assimilated, large RMSE reduction is concentrated within a relatively small radius surrounding each measurement location (Figs. 3a,c). By contrast, moving gliders extend the radius of influence and produce more uniform error reduction throughout the domain (Figs. 3b,d). Glider motion is predominantly responsible for this improvement, which is illustrated by running an additional experiment that follows G2.0, but assimilates only one profile per day (experiment G2.0D; Table 4). Comparing experiments F2.0, G2.0, and G2.0D, most of the additional RMSE reduction achieved by assimilating gliders results from platform motion (Table 5). Assimilating multiple profiles per day produces no additional RMSE reduction for D_{1000}, and produces only a small additional reduction for $T_{0–100}$ (Table 5).

The resulting localization of RMSE reduction around platform locations is illustrated in Fig. 4. RMSE reduction from experiments G2.0 and F2.0 are calculated as a function of radial distance from the location of each stationary platform, or the release point of each glider, and then averaged over all realizations of each platform type. RMSE reduction from stationary platforms is almost entirely confined within ~50 km of

TABLE 5. RMSE and percent reduction in RMSE for D_{1000} and $T_{0–100}$ with respect to the FM for experiment F2.0, G2.0, and another experiment similar to G2.0 but assimilating only one profile per day.

Field	Expt	RMSE	% reduction
D_{1000}	Unconstrained FM	0.103	
	F2.0	0.096	6
	G2.0	0.072	30
	G2.0D	0.072	30
$T_{0–100}$	Unconstrained FM	0.777	
	F2.0	0.719	7
	G2.0	0.527	32
	G2.0D	0.559	28

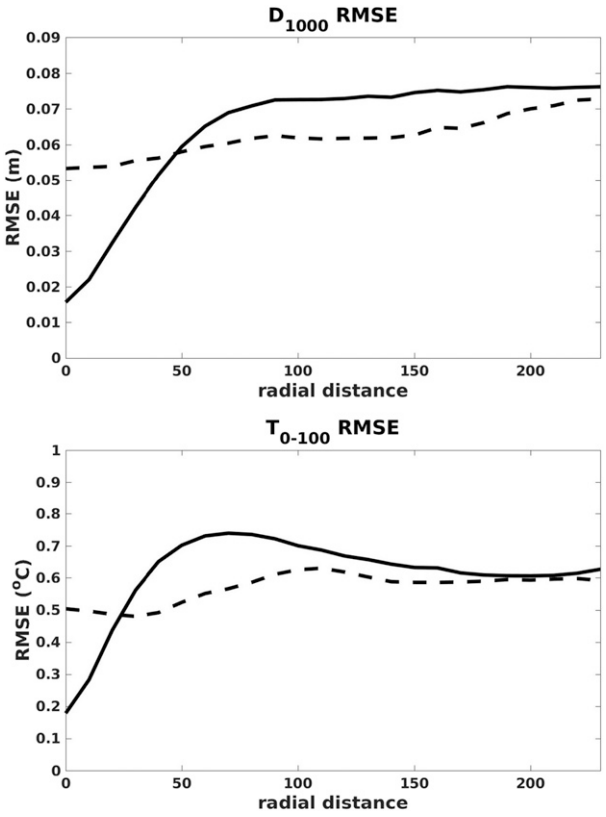

FIG. 4. RMSE in (top) D_{1000} and (bottom) $T_{0–100}$ graphed as a function of radial distance from measurement points. Solid and dashed curves are for fixed-location measurements and gliders, respectively. RMSE values at model grid points surrounding each measurement location for stationary profilers (each release point for gliders) are binned according to radial distance from that point, with bins set to 0–5, 5–15, 15–25, . . . , 225–235 km. Mean RMSE was then calculated for each radial bin.

measurement points, slightly larger for D_{1000} than for $T_{0–100}$. By contrast, RMSE reduction achieved by gliders is much more uniform with distance from the release point (Fig. 4). Although RMSE reduction is smaller in the vicinity of the release point due to glider motion, it is larger for D_{1000} over radial distances from 50 to at least 230 km and is larger for $T_{0–100}$ over radial distances from 30 to 175 km. Although the larger RMSE reduction produced by gliders at larger radii is modest compared to the larger RMSE produced by stationary platforms at small radii, the differences at larger radii dominate because they represent a larger surface area. This not only leads to more uniform RMSE reduction, but also to a larger RMSE reduction throughout the domain, by moving gliders.

To understand why glider motion produces significant additional RMSE reduction, the primary factors that limit the radius of influence of assimilated ocean profiles are investigated. First, limitations in the DA procedure reduce the accuracy of analysis increments with increasing distance from platform locations. Second, rapid error growth away from platform locations occurs due to nonlinear advection by energetic mesoscale eddies.

b. *Influence of DA procedure*

To illustrate the influence of limitations in the DA procedure, the error of $T_{0–100}$ from experiment F2.0, defined as the difference FM minus NR, is compared to the analysis increments realized during the first update cycle (2 May). Negative error (NR minus FM) is plotted in Fig. 5a because it illustrates the perfect correction pattern that would reduce error to zero. The analysis increment field (Fig. 5d) demonstrates that the analysis introduces unrealistic mesoscale structure due to the limited radius of influence of each assimilated profile. Focusing in more detail on individual sampling locations, Figs. 5b and 5e show the negative of the error field and the analysis increment around a single profile location. In this case, the increment has the correct sign everywhere within the localization radius to reduce error, but the rapid taper to zero reduces the accuracy of error reduction at larger radii. Figures 5c and 5f show a more extreme case where the analysis increment is not always of the same sign as the negative of the error field due to the presence of smaller-scale error structure. Profile assimilation actually increases error at some locations in the vicinity of this profiler. These results also apply to moving platforms when only one analysis cycle is considered.

Two properties of the DA procedure contribute to the limited accuracy and limited radius of influence of the increments. First, innovations at platform locations are spread by the background error covariance matrix, which tends to smooth the structure of the increments (e.g., Jacobs et al. 2014). Second, the radius of influence of each profiler is limited by tapering innovations away from observation locations by the Gaspari and Cohn (1999) localization radius function. Although increasing

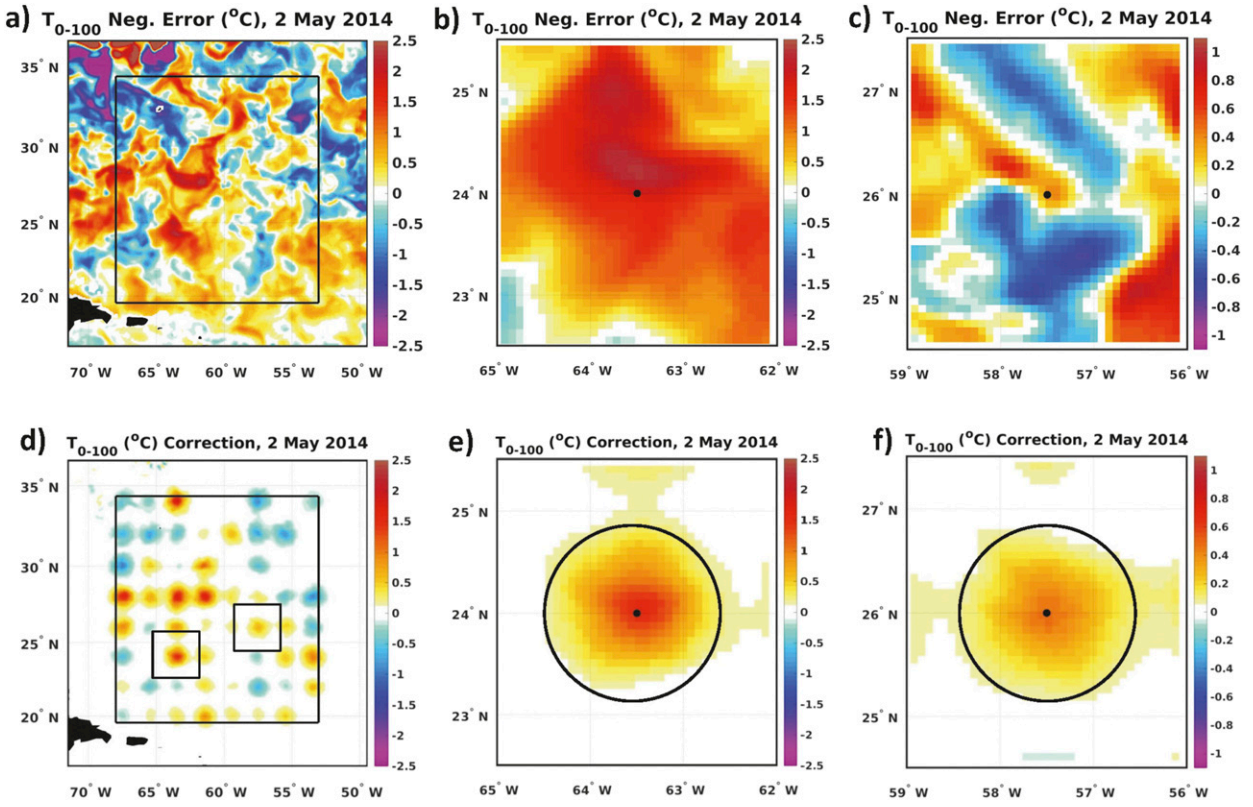

FIG. 5. Maps of negative error in $T_{0–100}$ within a domain surrounding the analysis box from experiment (a) F2.0 and (b),(c) surrounding two measurement locations on 2 May just before the first analysis is performed. Increments on the first analysis day (2 May) (d) within a domain surrounding the analysis box and (e),(f) surrounding two measurement locations. The two measurement locations are highlighted in (d).

the chosen radius of 200 km will admit more observations and tend to reduce the granularity of the increments in Fig. 5d, the inclusion of more distant observations that are poorly correlated with the analysis location will tend to reduce the accuracy of the resulting analysis. By contrast, reducing the radius will decrease the number of observations, increase the granularity of the increments, and eventually reduce analysis accuracy. The impact of this trade-off was tested by running variations of experiment F2.0 using both smaller and larger radii. The largest reduction in RMSE over the analysis domain was achieved using the 200-km radius (not shown), verifying the present choice.

c. *Influence of nonlinear advection*

The second factor (nonlinear advection) further limits the radius of influence. This impact is illustrated by inspecting daily time series of RMSE calculated over the analysis box (Fig. 1) of $T_{0–100}$ over the first month (May 2014) from several experiments that assimilated only gliders or stationary profilers (Fig. 6a). The additional RMSE reduction produced by moving gliders compared to fixed platform measurements when both platform types are deployed at the same horizontal resolution is evident. For both measurement types, rapid RMSE reduction is achieved over the first two daily analysis cycles, with gliders producing only slightly larger reduction at the same deployment resolution. This initial RMSE reduction is maintained by the gliders, but values for the stationary profiler experiments begin to grow after day four and continue to grow for the next ~17 days when they are deployed at intermediate (1°–2°) horizontal resolution (experiments F1.0 and F2.0). This secondary error growth is substantially responsible for reducing the radius of influence in comparison with moving gliders.

To demonstrate that nonlinear processes are primarily responsible for this error growth, the cumulative correction to the FM resulting from stationary profiler assimilation (experiment F2.0) is shown after nine daily analysis cycles (10 May; Fig. 6b). This cumulative correction contains the increments added during each cycle plus the model forecast evolution between each cycle. By this time, horizontal advection within the energetic mesoscale eddy field has greatly distorted the cumulative correction (cf. Figs. 6b and 4d) so that it is dominated by smaller-scale structure and filaments. The fact

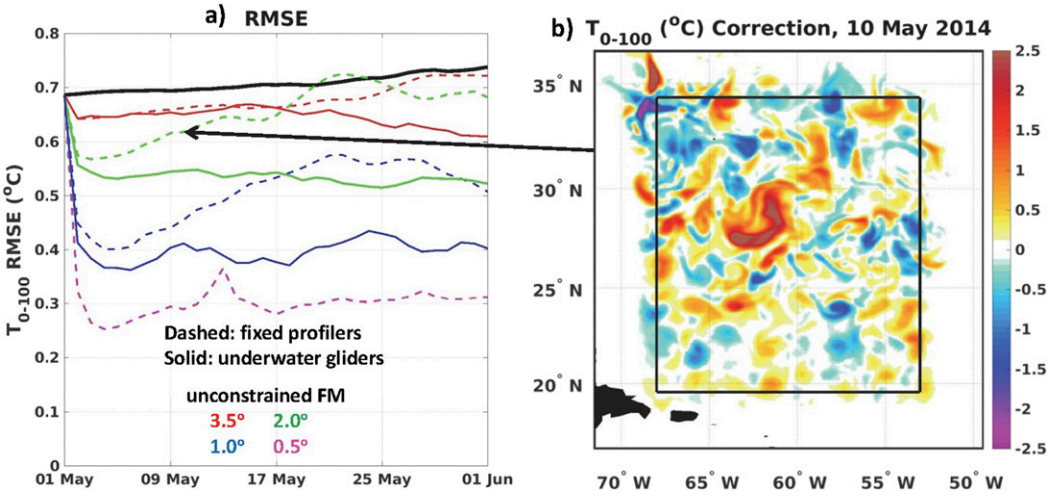

FIG. 6. (a) Time series of RMS errors in $T_{0–100}$ over the first month of several experiments in which platforms were deployed at high and intermediate resolution that assimilated only gliders (solid lines) or stationary profilers (dashed lines). Colors indicate instrument separation distances of 0.5° (magenta), 1.0° (blue), 2.0° (green), and 3.5° (red). The thick black curve represents the unconstrained FM. Also shown is (b) the cumulative correction (sum of all increments plus model forecasts) for $T_{0–100}$ from experiment F2.0 after nine analysis cycles. The arrow points to the time along the dashed green curve in (a) corresponding to the cumulative correction map.

that glider movement suppresses this error growth suggests that the ability to cross gradients and map a subset of the analysis domain substantially counters the impact of nonlinearity.

The situation is substantially different for D_{1000}. Correcting the surface pressure field associated with mesoscale features requires correcting the ocean density distribution over the full depth range of the features. Because horizontal advection of the ocean thermal field weakens with depth, the impact of nonlinear advection on D_{1000} is weaker than on the upper-ocean thermal field. The resulting situation is illustrated by the RMSE evolution for D_{1000} during the first month from several experiments (Fig. 7). When glider and fixed-location profiles are deployed at high horizontal resolution (experiments G1.0, F0.5, and F1.0), rapid RMSE reduction is realized over the first three days, and this reduction is substantially maintained at longer times. By contrast, both stationary profilers and gliders sampling at lower horizontal resolutions of 2.0° and 3.5° (experiments F2.0, F3.5, G2.0, and G3.5) produce small error reduction over the first three days. After that time, this minimal error reduction is maintained by stationary profilers while gliders produce a slow decrease in error over the first month. Gliders deployed at intermediate resolution therefore require an extended period of time to gradually map the three-dimensional structure of the density field associated with mesoscale features. Because of this property, seasonal glider arrays with intermediate resolution should be deployed at least one month prior to the start of hurricane season.

6. Quantitative impact assessments

a. *RMS error reduction*

RMSE values for all experiments assimilating only gliders and stationary profilers, and for the six model

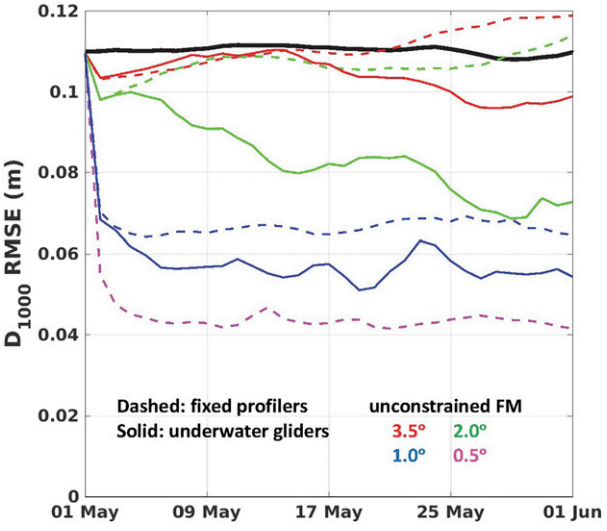

FIG. 7. Time series of daily RMSE values for D_{1000} over the first month from several experiments in which platforms are deployed at high and intermediate resolution. Colors indicate instrument separation distances of 0.5° (magenta), 1.0° (blue), 2.0° (green), and 3.5° (red). The thick black curve represents the unconstrained FM.

fields analyzed, are calculated by averaging daily estimates between 1 July and 12 October 2014. The percentage error reduction with respect to the unconstrained FM is then calculated and presented in bar graphs (Fig. 8). In all cases, error reduction for gliders is larger than for stationary profilers for each horizontal separation distance. The error reduction for large separation distances is minimal for the three upper-ocean thermal fields (SST, T_{100}, and $T_{0–100}$) with no detectable improvement for separation distances $\geq$4.7° for both gliders and stationary profilers (experiments F4.7, F7.0, G4.7, and G7.0). Modest improvement for these there fields is detected for gliders at 3.5° separation (experiment G3.5). Otherwise, gliders need to be separated by 2.0° or less and stationary profilers need to be separated by 1.0° or less to consistently produce substantial error reduction. By contrast to the three upper-ocean thermal fields, RMSE reduction for D_{1000}, H_{20}, and SSS is generally detectable at separation distances of 3.5° and larger, particularly for SSS, which is generally inaccurately represented in unconstrained models.

It is also important to assess the additional positive impacts realized by assimilating moving and stationary profilers over assimilating components of the global ocean observing system. The percentage error reduction with respect to the unconstrained FM is presented in Fig. 9 for all experiments that add glider and stationary profiler assimilation to CONTROL. The black bars in all panels show the percentage RMSE reduction achieved by assimilating the components of the global ocean observing system. The color bar extensions then show the additional improvement achieved by assimilating gliders and stationary profilers. Again, the error reduction for gliders is larger than for stationary profilers for each horizontal separation distance. Only small additional improvement is achieved in D_{1000} for both gliders and stationary profilers, and only when the instruments are deployed at very high resolution (1.0° or less; experiments CF0.5, CF1.0, and CG1.0). Given the large correction in mesoscale structure provided by altimeters, platforms must be deployed at high horizontal resolution to correct the smaller scales that are not effectively corrected by altimetry. Modest additional improvement extends to larger separation distances for H_{20} and the three upper-ocean thermal fields.

For SSS, additional RMSE reduction is greater and extends to larger separation distances. Both gliders and stationary profilers effectively reduce SSS RMSE because errors are large in the unconstrained model and only partly corrected by altimetry and Argo. The Argo impact is demonstrated by comparing the larger RMSE reduction from CONTROL in the impact assessment experiments (Table 4; Fig. 9f) to the RMSE reduction from the OSSE system evaluation CONTROL experiment (Table 2; OSSE results in Fig. 2f), which is identical to the previous experiment except that Argo was withheld.

b. *Large-scale bias reduction*

Bar graphs of the percentage reduction in bias magnitude $|B|$ are presented for all model fields for experiments that assimilated gliders and stationary profilers alone (Fig. 10), and that added gliders and stationary profilers to CONTROL (Fig. 11). It is immediately clear that bias reduction remains large for all fields even as instrument separation (both stationary profilers and gliders) increases to 7.0°. For both platform types, the radius of influence for large-scale bias correction (several hundred kilometers) is much larger than for RMSE correction, with moving gliders having slightly larger impact. Nonlinear advection limits the radius of influence for RMSE, but it apparently acts to spread bias correction achieved near platform locations over much longer distances.

c. *Error reduction in horizontal mesoscale structure*

Although RMSE reduction was analyzed to study impacts on correcting mesoscale variability, it is also instructive to analyze impacts on correcting horizontal mesoscale structure. Power spectra are calculated in zonal and meridional wavenumber space using a maximum entropy method available in the MATLAB software package (Burg's algorithm; Burg 1975). Space–time averaging is performed in lieu of averaging over wavenumber space to increase degrees of freedom while preserving the full range of resolved wavelengths at the highest possible resolution. For zonal wavenumber, these functions are computed separately along each meridional grid row in the analysis box (Fig. 1), averaged over all grid rows on each day, and finally averaged over time. For meridional wavenumber, these functions are computed separately along each zonal grid column in the analysis box, averaged over all grid columns on each day, and finally averaged over time. Because the model gridpoint spacing $dx = dy$ in kilometers decreases as the cosine of latitude in the Mercator mesh, all spectrum functions are calculated assuming that both dx and dy equal the grid spacing at the central latitude of the box. The resulting distortion in autospectrum and cross-spectrum functions in wavenumber space is minor and does not significantly affect analysis results. The resulting autospectra are resolved over the range of wavelengths from the Nyquist values of the FM mesh (~15 km) to ~1450 km. Wavelengths <80 km are excluded from all spectrum plots because insignificant error reduction

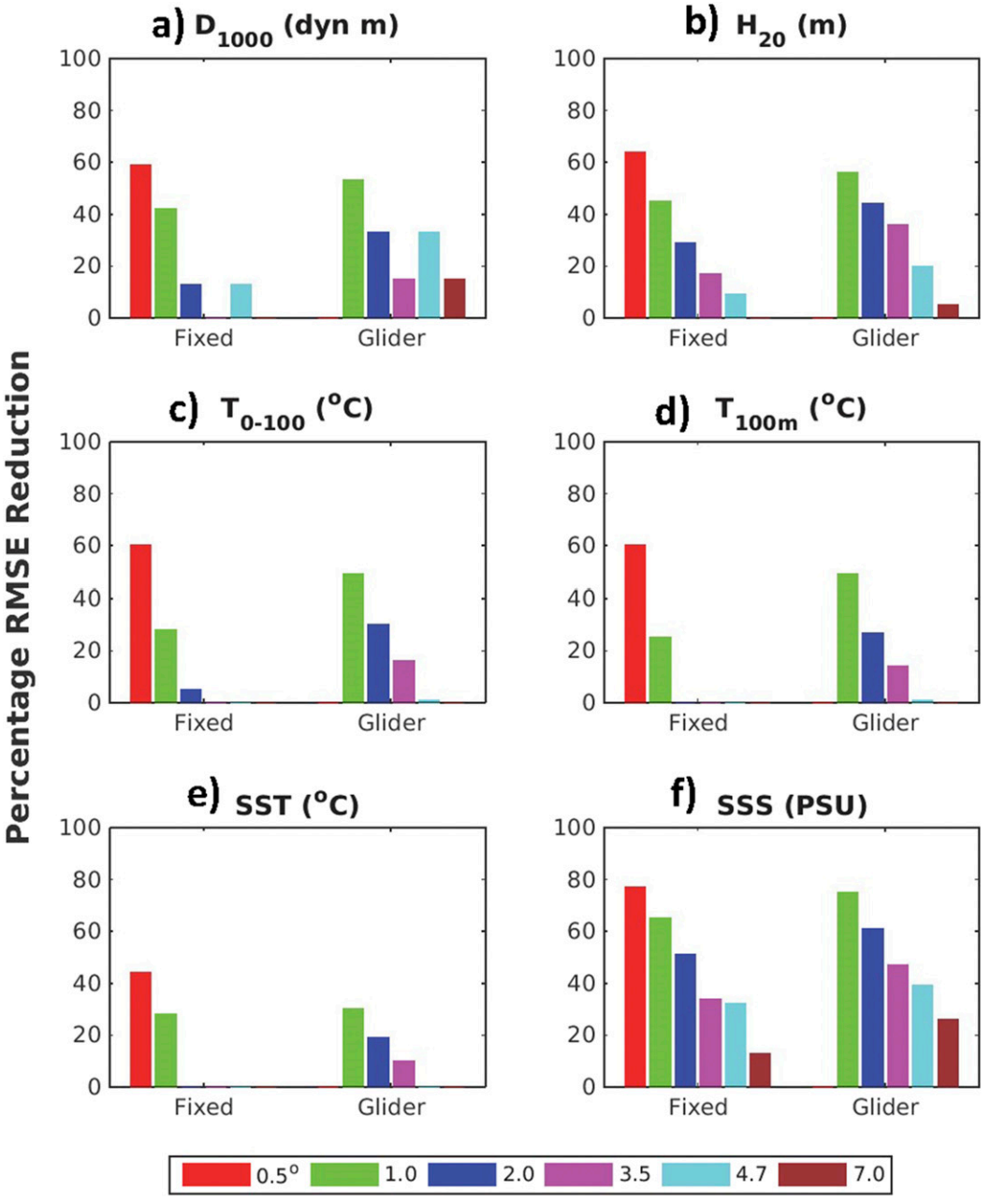

FIG. 8. Percentage reduction in RMSE for six model fields calculated over the time interval 1 Jul–12 Oct 2014 for all experiments that assimilated only gliders or stationary profilers.

is achieved over this range. Zonal and meridional wavenumber spectra are presented for D_{1000} and $T_{0–100}$ for all glider and stationary profiler experiments with horizontal separations of 3.5° or less.

The spectra for experiments assimilating either gliders or stationary profilers alone are presented in Fig. 12. The additional correction provided by gliders over fixed-location measurements is evident at all separation distances. For stationary profilers, error reduction in both fields is confined to wavelengths exceeding the Nyquist, defined as twice the nominal separation distance among instruments. Over smaller wavelengths, errors actually increase for both fields, presumably resulting from the introduction of unphysical structure by the daily increments (see Fig. 5d). Not only does glider assimilation further reduce errors over fixed platform measurements, but error reduction extends to smaller wavelengths due to the ability of

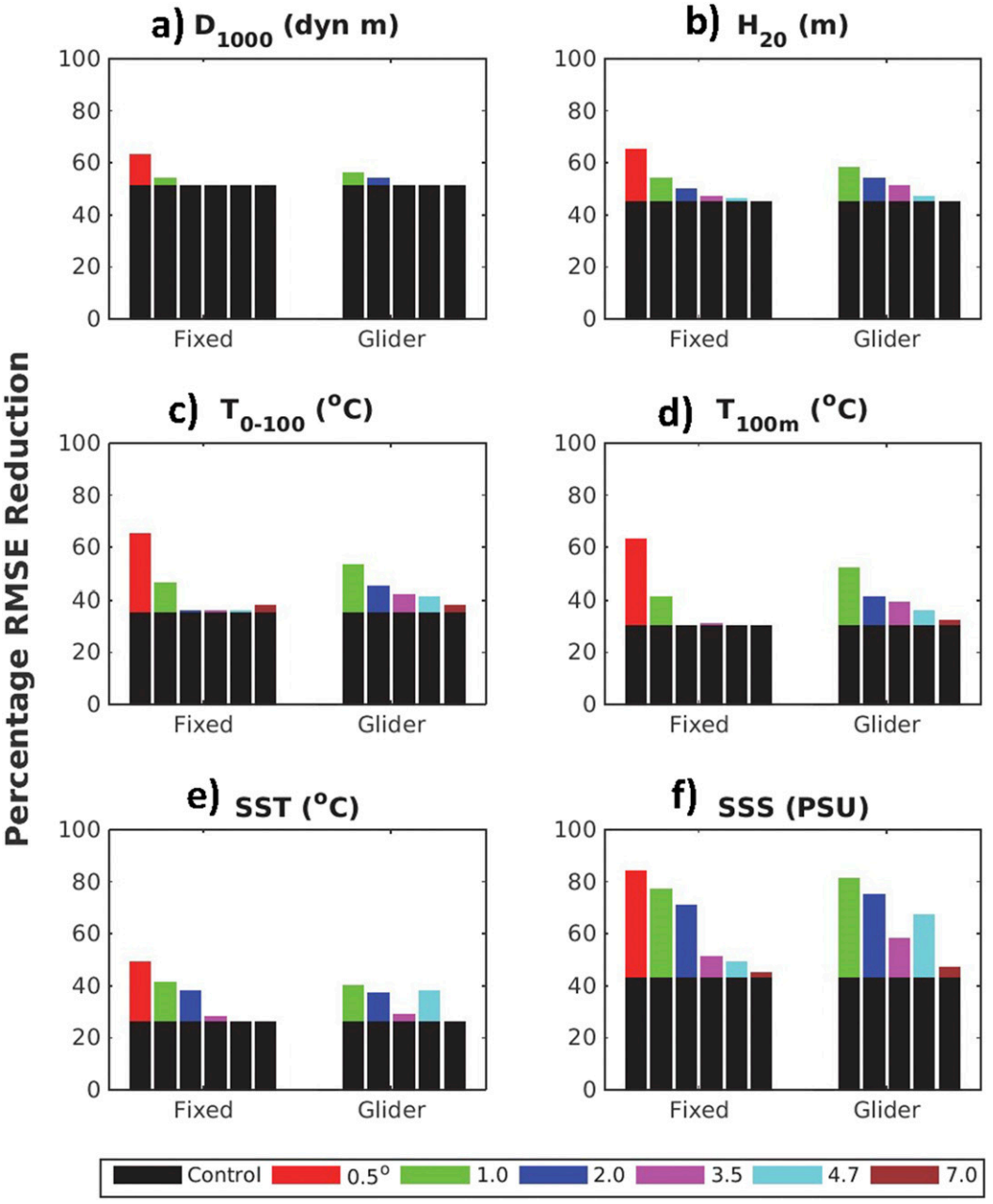

FIG. 9. Percentage reduction in RMSE for six model fields calculated over the time interval 1 Jul–12 Oct 2014 for all experiments that added gliders or stationary profilers to CONTROL.

each glider to cross gradients and map mesoscale structure over its own subregion.

The wavenumber spectra for experiments assimilating either gliders or stationary profilers added to CONTROL are presented in Fig. 13. In this case, impacts are measured as further improvement in mesoscale structure over CONTROL, which produces error reduction down to wavelengths of ~150 km. Again, improvement is greater for the gliders compared to fixed-platform measurements for the same horizontal separation. The additional improvement is substantially larger for $T_{0–100}$ than for D_{1000}, demonstrating the effectiveness of satellite altimetry at improving the three-dimensional structure of mesoscale features. However, altimetry is less effective at correcting the thermal field over the upper 100 m of the ocean associated with these features. The ability of gliders separated by $\leq 2.0°$ and stationary profilers separated by $\leq 1.0°$ to provide substantial additional correction

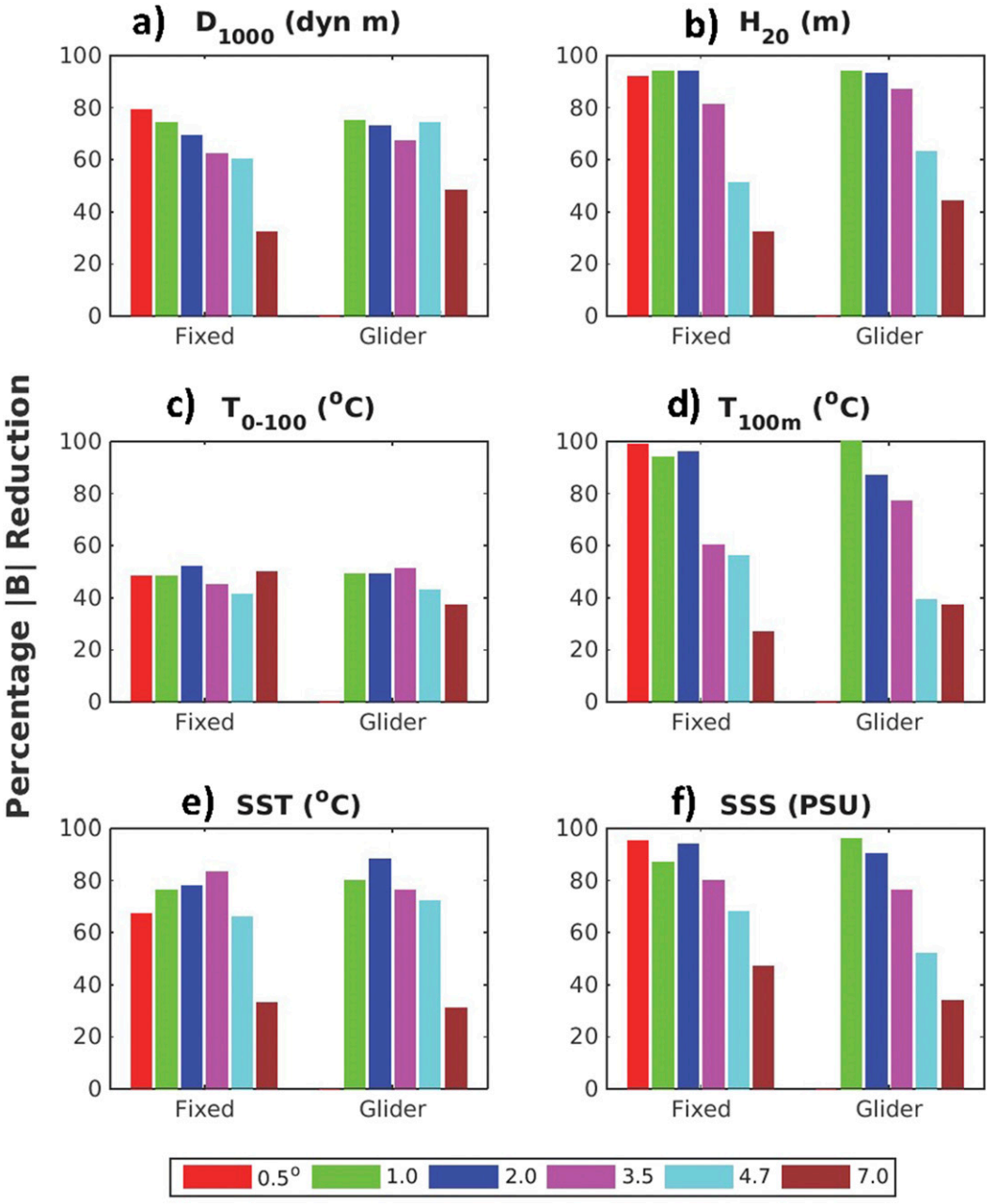

FIG. 10. Percentage reduction in bias magnitude $|B|$ for six model fields calculated over the time interval 1 Jul–12 Oct 2014 for all experiments that assimilated only gliders or stationary profilers.

to upper-ocean thermal fields is valuable for TC prediction applications.

7. Conclusions and recommendations

A regional ocean OSSE system for the western North Atlantic was used to quantitatively assess the impact of seasonally deployed arrays of underwater gliders on improving ocean forecast model initialization, with particular attention paid to improving coupled TC prediction. The latest updates to the OSSE system configuration were described and evaluated. The advantages of assimilating profiles collected from moving platform arrays, such as underwater gliders, over profiles collected from arrays of stationary platforms based on RMSE and bias reduction were demonstrated. For stationary platforms, significant RMSE reduction is primarily confined to within ~50 km of

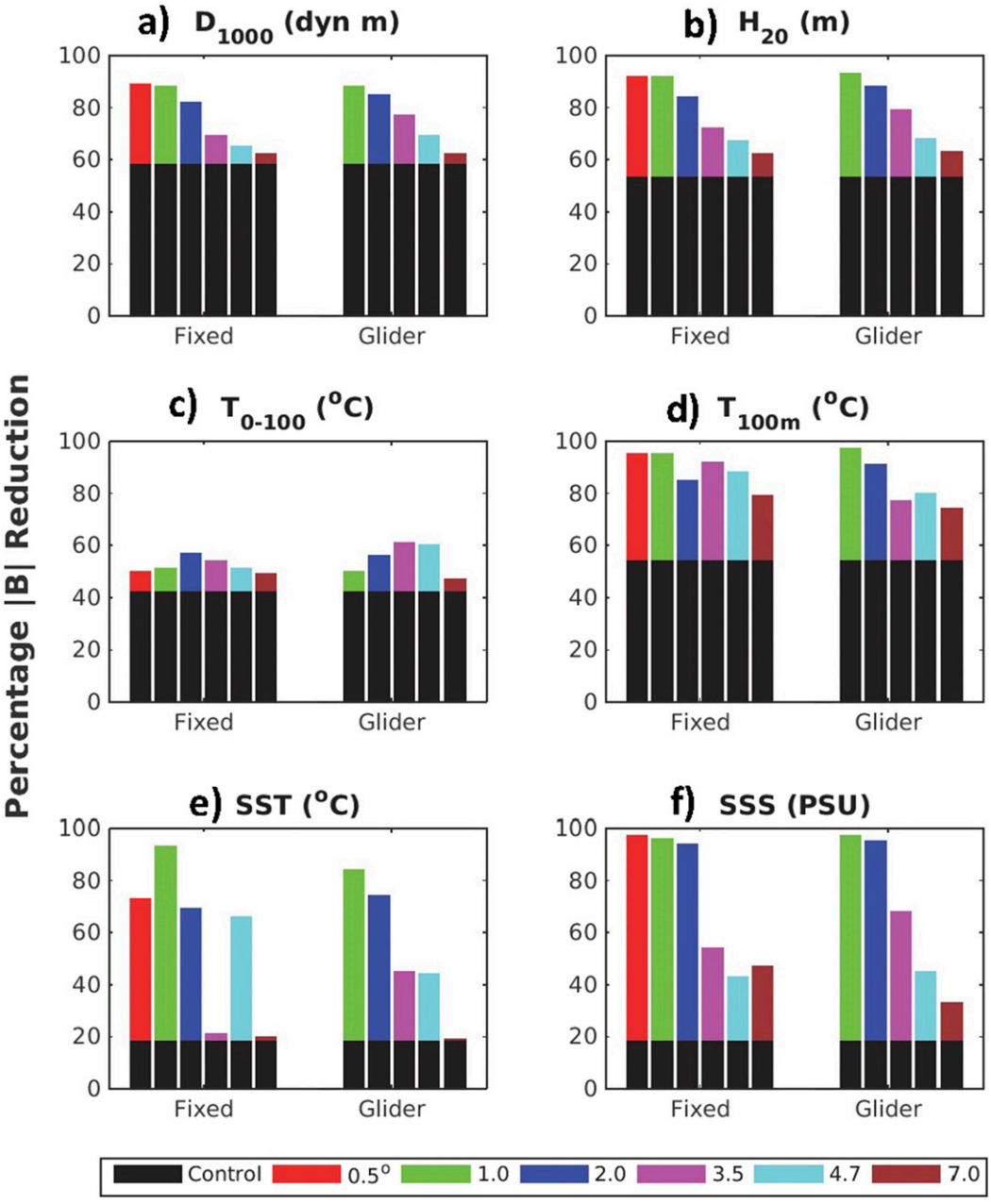

FIG. 11. Percentage reduction in $|B|$ for six model fields calculated over the time interval 1 Jul–12 Oct 2014 for all experiments that added gliders or stationary profilers to CONTROL.

measurement locations, with this radius being slightly larger for the upper-ocean pressure field represented by D_{1000} than for the upper-ocean thermal field represented by $T_{0\text{–}100}$. Stationary platforms must therefore be deployed at high horizontal resolution ($\leq 1°$) to provide significant correction of ocean mesoscale structure. This is particularly true when these ocean profiles are assimilated in addition to the existing global ocean observing system, including altimetry, which already substantially corrects mesoscale structure.

Compared to stationary platforms, arrays of moving gliders are more effective at reducing RMSE in model fields. Modest error reduction in mesoscale variability due to gliders is achieved with nominal spacing of 3.5° while substantially larger error reduction is achieved at 2.0° separation, the latter approaching the reduction achieved by stationary platforms with nominal spacing of 1.0°. Wavenumber spectrum analysis demonstrates that error reduction in horizontal mesoscale structure

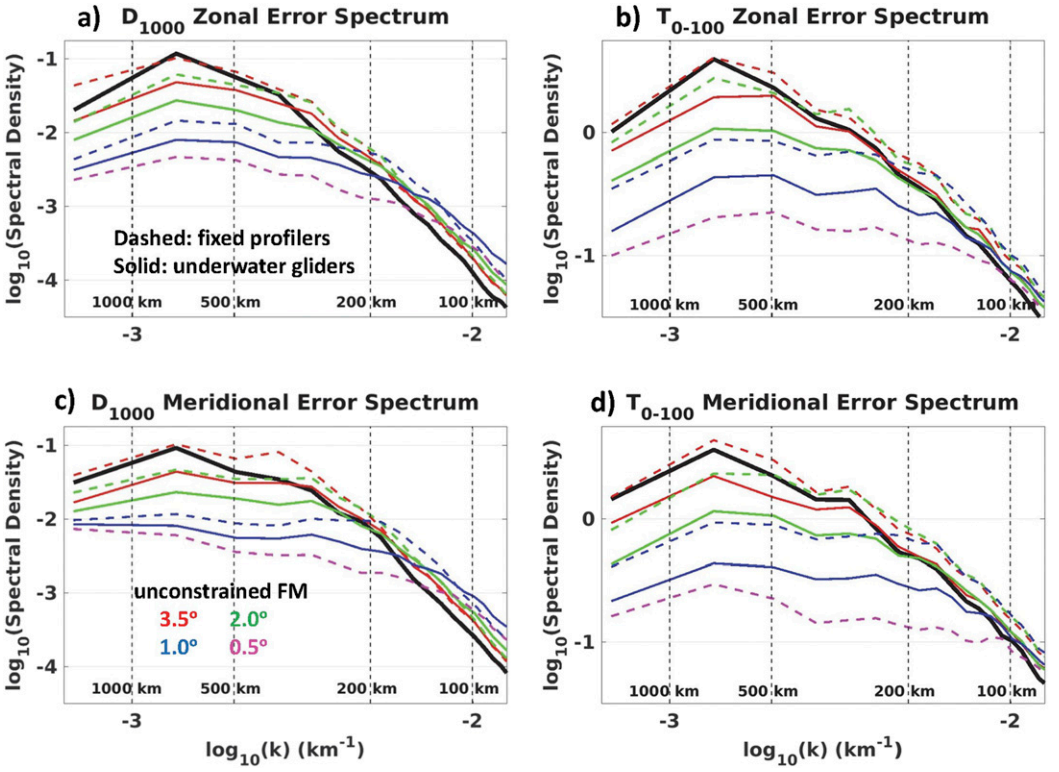

FIG. 12. Wavenumber spectrum error analysis for (left) D_{1000} and (right) $T_{0–100}$ from experiments in which platforms were deployed at high and medium resolution that quantitatively assess the impact of assimilating gliders and stationary profilers alone; (top) zonal and (bottom) meridional spectra are shown.

achieved by assimilating moving gliders extends to smaller wavelengths compared to assimilating profiles from stationary platforms. These differences have a large impact on the number of platforms required to achieve a predetermined level of error reduction within a predefined ocean region. For example, a $6° \times 6°$ ocean region can be sampled by around 9 gliders to achieve nominal 2° separation. Based on present analysis results, at least 20 stationary profilers need to be deployed in that same region to achieve equal or greater error reduction. Piloted gliders therefore have a significant advantage for reducing mesoscale error.

The situation is different for the correction of large-scale bias in initial ocean fields. Both platform types can be deployed at much coarser resolution, separated by up to several hundred kilometers, and still significantly reduce large-scale bias, with moving gliders being modestly more effective. If bias reduction is the only goal, a small number of platforms, stationary or moving, can be deployed over a very large ocean area. However, accurate SST forecasts by coupled TC prediction models still require accurate initialization of mesoscale structure.

Even with the advantages documented herein, it will be difficult to rely on gliders alone to improve TC prediction over large ocean regions due to the large numbers that will be required. An optimum strategy will likely involve the strategic deployment of gliders supplemented by rapid-response ocean measurement programs involving prestorm airborne ocean profiler surveys and prestorm deployments of in situ ocean profiling floats as needed. Future OSSEs will need to be performed to design and evaluate such measurement strategies.

The high-resolution, three-dimensional representation of the truth provided by the OSSE system NR, are exploited to investigate important factors that limit RMSE reduction and affect impact assessments documented herein. Each daily update cycle tends to introduce unphysical eddy structure due to smoothing properties of the background error covariance matrix, and also due to the tapering of analysis increments to zero within a radius of 200 km by the Gaspari and Cohn (1999) localization function. Furthermore, rapid error growth occurs due to nonlinear advection in this eddy-rich region, particularly for near-surface thermodynamical fields. When ocean profiles collected at fixed locations are assimilated, these factors collectively limit the radius surrounding each profiler location where

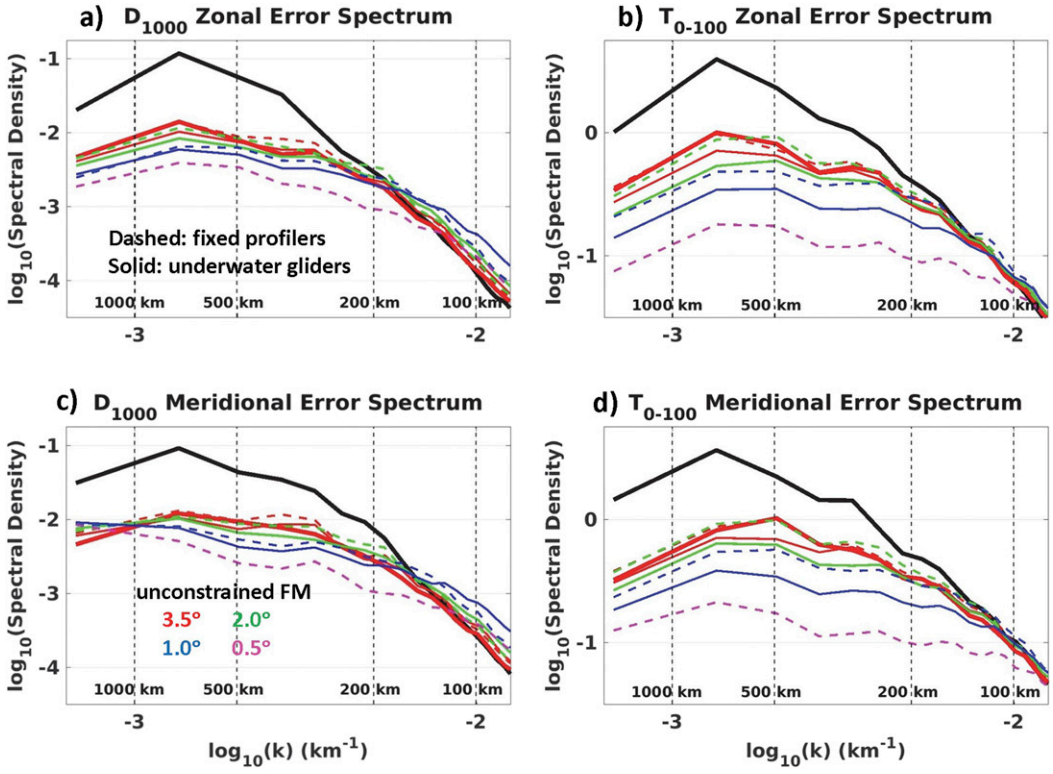

FIG. 13. Wavenumber spectrum error analysis for (left) D_{1000} and (right) $T_{0–100}$ from experiments in which platforms were deployed at high or intermediate resolution that quantitatively assess the impact of adding gliders and stationary profilers to CONTROL; (top) zonal and (bottom) meridional spectra are shown.

RMSE reduction is achieved. By contrast, the ability of moving gliders to cross gradients and map mesoscale structure in their vicinity substantially reduces nonlinear error growth, allowing an array of gliders to produce a more-uniform RMSE reduction over the deployment region.

When ocean profile assimilation is initiated, RMSE in upper-ocean thermal fields rapidly decreases over the first three days for both stationary and moving platforms. For stationary platforms, RMSE in upper-ocean thermal fields then increases over the next 2–3 weeks as advection distorts the correction field, which significantly reduces the steady-state RMSE reduction achieved after the error growth. By contrast, this RMSE growth does not occur when profiles from moving gliders are assimilated. Apparently, the mapping capability of individual moving gliders over the subregion that they sample more effectively reduces errors in the representation of mesoscale ocean features.

Nonlinear advection has a more limited effect on the correction of the three-dimensional pressure field associated with mesoscale features. This pressure distribution depends on the density distribution over the full depth range of these features [O(1000) m] while horizontal advection of temperature and salinity is primarily confined to the surface mixed layer and seasonal thermocline [O(100) m]. When ocean profile assimilation is initiated, RMSE rapidly decreases over the first three days for both stationary and moving platforms as observed for thermal fields. Continued assimilation of profiles from stationary platforms maintains this reduced RMSE. However, continued assimilation of profiles from moving gliders produces a further steady decrease in RMSE over the next month when deployed at intermediate horizontal resolution (between 2.0° and 3.5°). The mapping ability of each moving glider slowly improves the representation of the three-dimensional pressure field associated with mesoscale features. Consequently, glider arrays deployed at intermediate separation distances need to be deployed at least one month prior to the start of hurricane season for maximum impact. This ability to quantify the influence of nonlinear advection on observing-system impacts is a significant advantage of OSSE systems over linearized procedures such as adjoint methods.

Limitations to these results must be considered. Results are strictly valid only for the western North Atlantic region that was studied. Other regions with

different levels of mesoscale variability will produce different quantitative results. More importantly, OSSE results depend on the properties of the OSSE system, in particular the DA methodology used. The present study must therefore be considered as an initial documentation of the expected improvements that will result from assimilating profiles from moving versus stationary platforms deployed at different horizontal resolutions. The impact of nonlinear advection documented herein will affect the accuracy of ocean analyses produced by other ocean prediction systems that use different DA methodology. All DA systems enforce some form of localization that limits the effective radius of influence of each individual observation. It is possible that more advanced DA methods such as 3DVAR and 4DVAR will produce larger error and bias reduction. Analyses presented herein should be repeated in different ocean regions using different DA systems, including those used by operational centers, to document the robustness of these results.

Acknowledgments. The authors acknowledge the support from the NOAA Quantitative Observing System Assessment Program (QOSAP; OAR-P8R2W02PQF and NA15OAR4320064). Authors G. Halliwell and M. Mehari acknowledge internal support from the NOAA/AOML/Physical Oceanography Division. The authors acknowledge the NOAA Research and Development High Performance Computing Program (http://rdhpcs.noaa.gov) for providing computing and storage resources that have contributed to the research results presented in this paper.

REFERENCES

Androulidakis, Y., V. Kourafalou, G. Halliwell, M. Le Hénaff, H. Kang, M. Mehari, and R. Atlas, 2016: Hurricane interaction with the upper ocean in the Amazon-Orinoco plume region. *Ocean Dyn.*, **66**, 1559–1588, https://doi.org/10.1007/s10236-016-0997-0.

Atlas, R., 1997: Atmospheric observations and experiments to assess their usefulness in data assimilation. *J. Meteor. Soc. Japan*, **75**, 111–130, https://doi.org/10.2151/jmsj1965.75.1B_111.

——, and L. P. Riishojgaard, 2008: Application of OSSEs to observing system design. *Proc. SPIE*, **7087**, 708707, https://doi.org/10.1117/12.795344.

Bleck, R., 2002: An oceanic general circulation model framed in hybrid isopycnic-Cartesian coordinates. *Ocean Modell.*, **4**, 55–88, https://doi.org/10.1016/S1463-5003(01)00012-9.

Burg, J. P., 1975: Maximum entropy spectral analysis. Ph.D. dissertation, Stanford University, 123 pp.

Chassignet, E. P., L. T. Smith, G. R. Halliwell, and R. Bleck, 2003: North Atlantic simulation with the Hybrid Coordinate Ocean Model (HYCOM): Impact of the vertical coordinate choice, reference density, and thermobaricity. *J. Phys. Oceanogr.*, **33**, 2504–2526, https://doi.org/10.1175/1520-0485(2003)033<2504:NASWTH>2.0.CO;2.

——, H. E. Hurlburt, O. M. Smedstad, G. R. Halliwell, P. J. Hogan, A. J. Wallcraft, and R. Bleck, 2007: Ocean prediction with the Hybrid Coordinate Ocean Model (HYCOM). *J. Mar. Syst.*, **65**, 60–83, https://doi.org/10.1016/j.jmarsys.2005.09.016.

Cooper, M., and K. Haines, 1996: Altimetric assimilation with water property conservation. *J. Geophys. Res.*, **101**, 1059–1077, https://doi.org/10.1029/95JC02902.

Domingues, R., and Coauthors, 2015: Upper ocean response to Hurricane Gonzalo (2014): Salinity effects revealed by sustained and targeted observations from underwater gliders. *Geophys. Res. Lett.*, **42**, 7131–7138, https://doi.org/10.1002/2015GL065378.

Dong, J., and Coauthors, 2017: Impact of assimilating underwater glider data on Hurricane Gonzalo (2014) forecast. *Wea. Forecasting*, **32**, 1143–1159, https://doi.org/10.1175/WAF-D-16-0182.1.

Gaspari, G., and S. E. Cohn, 1999: Construction of correlation functions in two and three dimensions. *Quart. J. Roy. Meteor. Soc.*, **125**, 723–757, https://doi.org/10.1002/qj.49712555417.

Goni, G., and Coauthors, 2009: Applications of satellite-derived ocean measurements to tropical cyclone intensity forecasting. *Oceanography*, **22** (3), 190–197, https://doi.org/10.5670/oceanog.2009.78.

Halliwell, G. R., Jr., 2004: Evaluation of vertical coordinate and vertical mixing algorithms in the Hybrid-Coordinate Ocean Model (HYCOM). *Ocean Modell.*, **7**, 285–322, https://doi.org/10.1016/j.ocemod.2003.10.002.

——, L. K. Shay, S. D. Jacob, O. M. Smedstad, and E. W. Uhlhorn, 2008: Improving ocean model initialization for coupled tropical cyclone forecast models using GODAE nowcasts. *Mon. Wea. Rev.*, **136**, 2576–2591, https://doi.org/10.1175/2007MWR2154.1.

——, ——, J. Brewster, and W. J. Teague, 2011: Evaluation and sensitivity analysis of an ocean model response to Hurricane Ivan. *Mon. Wea. Rev.*, **139**, 921–945, https://doi.org/10.1175/2010MWR3104.1.

——, A. Srinivasan, V. Kourafalou, H. Yang, D. Willey, M. Le Hénaff, and R. Atlas, 2014: Rigorous evaluation of a fraternal twin ocean OSSE system in the open Gulf of Mexico. *J. Atmos. Oceanic Technol.*, **31**, 105–130, https://doi.org/10.1175/JTECH-D-13-00011.1.

——, V. Kourafalou, M. Le Henaff, R. Atlas, and L. K. Shay, 2015: OSSE impact analysis of airborne ocean surveys for improving upper-ocean dynamical and thermodynamical forecasts in the Gulf of Mexico. *Prog. Oceanogr.*, **130**, 32–46, https://doi.org/10.1016/j.pocean.2014.09.004.

——, M. Mehari, M. Le Henaff, V. H. Kourafalou, Y. S. Androulidakis, H-S. Kang, and R. Atlas, 2017a: North Atlantic Ocean OSSE system: Evaluation of operational ocean observing system components and supplemental seasonal observations for potentially improving coupled tropical cyclone prediction. *J. Oper. Oceanogr.*, **10**, 154–175, https://doi.org/10.1080/1755876X.2017.1322770.

——, ——, L. K. Shay, V. H. Kourafalou, H. Kang, H.-S. Kim, J. Dong, and R. Atlas, 2017b: OSSE quantitative assessment of rapid-response prestorm ocean surveys to improve coupled tropical cyclone prediction. *J. Geophys. Res. Oceans*, **122**, 5729–5748, https://doi.org/10.1002/2017JC012760.

Hoffman, R. N., and R. Atlas, 2015: Future observing system simulation experiments. *Bull. Amer. Meteor. Soc.*, **96**, 1601–1616, https://doi.org/10.1175/BAMS-D-15-00200.1.

Jacob, S. D., and L. K. Shay, 2003: The role of oceanic mesoscale features on the tropical cyclone induced mixed layer response. *J. Phys. Oceanogr.*, **33**, 649–676, https://doi.org/10.1175/1520-0485(2003)33<649:TROOMF>2.0.CO;2.

Jacobs, G. A., and Coauthors, 2014: Data assimilation considerations for improved ocean predictability during the Gulf of Mexico Grand Lagrangian Deployment (GLAD). *Ocean Modell.*, **83**, 98–117, https://doi.org/10.1016/j.ocemod.2014.09.003.

Jaimes, B., and L. K. Shay, 2009: Mixed layer cooling in mesoscale oceanic eddies during Hurricanes Katrina and Rita. *Mon. Wea. Rev.*, **137**, 4188–4207, https://doi.org/10.1175/2009MWR2849.1.

——, ——, and G. R. Halliwell, 2011: The response of quasigeostrophic vortices to tropical cyclone forcing. *J. Phys. Oceanogr.*, **41**, 1965–1985, https://doi.org/10.1175/JPO-D-11-06.1.

——, ——, and E. W. Uhlhorn, 2015: Enthalpy and momentum fluxes during Hurricane Earl relative to underlying ocean features. *Mon. Wea. Rev.*, **143**, 111–131, https://doi.org/10.1175/MWR-D-13-00277.1.

——, ——, and J. K. Brewster, 2016: Observed air-sea interactions in Tropical Cyclone Isaac over Loop Current mesoscale eddy features. *Dyn. Atmos. Oceans*, **76**, 306–324, https://doi.org/10.1016/j.dynatmoce.2016.03.001.

Kourafalou, V., Y. Androulikakis, G. R. Halliwell Jr., H. Kang, M. Mehari, M. Le Hénaff, R. Atlas, and R. Lumpkin, 2016: North Atlantic Ocean OSSE system development: Nature Run evaluation and application to hurricane interaction with the Gulf Stream. *Prog. Oceanogr.*, **148**, 1–25, https://doi.org/10.1016/j.pocean.2016.09.001.

Large, W. G., J. C. McWilliams, and S. C. Doney, 1994: Oceanic vertical mixing: A review and a model with a nonlocal boundary layer parameterization. *Rev. Geophys.*, **32**, 363–403, https://doi.org/10.1029/94RG01872.

Ma, Z., J. Fei, L. Liu, X. Huang, and X. Cheng, 2013: Effects of the cold-core eddy on tropical cyclone intensity and structure under idealized air–sea interaction conditions. *Mon. Wea. Rev.*, **141**, 1285–1303, https://doi.org/10.1175/MWR-D-12-00123.1.

Mellor, G. L., and T. Yamada, 1982: Development of a turbulence closure model for geophysical fluid problems. *Rev. Geophys. Space Phys.*, **20**, 851–875, https://doi.org/10.1029/RG020i004p00851.

Oke, P. R., and Coauthors, 2015: Assessing the impact of observations on ocean forecasts and reanalyses: Part 2: Regional applications. *J. Oper. Oceanogr.*, **8** (Suppl.), s63–s79, https://doi.org/10.1080/1755876X.2015.1022080.

Price, J. F., 2009: Metrics of hurricane-ocean interaction: Vertically integrated or vertically averaged ocean temperature? *Ocean Sci.*, **5**, 351–368, https://doi.org/10.5194/os-5-351-2009.

Scharroo, R., W. H. F. Smith, and J. L. Lillibridge, 2005: Satellite altimetry and the intensification of Hurricane Katrina. *Eos, Trans. Amer. Geophys. Union*, **86**, 366–367, https://doi.org/10.1029/2005EO400004.

Shay, L. K., G. J. Goni, and P. G. Black, 2000: Effects of a warm oceanic feature on Hurricane Opal. *Mon. Wea. Rev.*, **128**, 1366–1383, https://doi.org/10.1175/1520-0493(2000)128<1366:EOAWOF>2.0.CO;2.

——, and Coauthors, 2011: Airborne ocean surveys of the Loop Current complex from NOAA WP-3D in support of the *Deepwater Horizon* oil spill. *Monitoring and Modeling the Deepwater Horizon Oil Spill: A Record-Breaking Enterprise, Geophys. Monogr.*, Vol. 195, Amer. Geophys. Union, 131–151.

Turpin, V., E. Remy, and P. Y. Le Traon, 2016: How essential are Argo observations to constrain a global ocean data assimilation system? *Ocean Sci.*, **12**, 257–274, https://doi.org/10.5194/os-12-257-2016.

Verrier, S., P.-Y. Le Traon, and E. Remy, 2017: Assessing the impact of multiple altimeter missions and Argo in a global eddy-permitting data assimilation system. *Ocean Sci.*, **13**, 1077–1092, https://doi.org/10.5194/os-13-1077-2017.

Wu, C. C., C. Y. Lee, and I. I. Lin, 2007: The effect of the ocean eddy on tropical cyclone intensity. *J. Atmos. Sci.*, **64**, 3562–3578, https://doi.org/10.1175/JAS4051.1.